# Bimetallic Complexes in Zeolites: Reactivity of Tetracarbonyl(trimethylstannyl)cobalt in Acidic Zeolite Y

**Christian Huber, Karin Moller, Steven B. Ogunwumi, and Thomas Bein***

*Department of Chemistry, Purdue University, West Lafayette, Indiana 47907*

*Received: July 1, 1994; In Final Form: October 10, 1994*®

Stabilization techniques for low-valent organometallic species in acidic forms of large-pore zeolite Y are reported. The intrazeolite surface chemistry and thermal stability of $Me_3SnCo(CO)_4$ in HY zeolites ($H_{45}Na_{10}Al_{55}Si_{137}O_{384}$ and $H_{16}Na_{39}Al_{55}Si_{137}O_{384}$) were studied with X-ray absorption spectroscopy (Sn, Co edge EXAFS) and *in-situ* FTIR/TPD-MS techniques. The acidic zeolite Y host offers a chemically reactive surface that can interact with the $Me_3Sn$ moiety of the bimetallic complex. FTIR and EXAFS data indicate attachment of the complex to the zeolite framework. The intrazeolite SnCo complex is accessible toward carbonyl substitution with $PMe_3$. One observes growing attachment of the precursor (progressive substitution of methyl ligands at tin) to the zeolite with increasing temperature, while the Sn−Co bond and the Co−carbonyl moiety remain stable up to about 90 °C. At higher temperatures the Sn−Co bond is cleaved, the carbonyl ligands are dissociated, and cobalt is oxidized in a reaction with the zeolite protons. The resulting cobalt ions attach to the zeolite framework. Infrared/TPD studies show that the SnCo complex reacts differently in the HY zeolite when containing only 16 protons per unit cell and that its decomposition results in metal clusters.

## Introduction

The preparation and reactivity of hybrid catalysts combining organometallic molecular species with a solid support structure continues to be of great interest.[1] One anticipates that facile product separation, flexibility in the choice of reactant medium, and stability of heterogeneous systems could be combined with the high selectivity and activity of some organometallic catalysts. Hybrid catalysts have often been employed for olefin hydrogenation, but also for reactions such as olefin hydroformylation, hydrosilylation, dimerization, and metathesis.[2] Typically, amorphous supports such as polystyrene or silica have been used.

When the catalytic centers are encapsulated in crystalline, microporous hosts such as zeolites,[3] catalytic selectivity could be enhanced by controlling access and transport of reactants and products in the catalyst pores. Zeolites are the archetypical crystalline porous inorganic hosts with pore dimensions spanning now 3−30 Å and beyond.[4] The well-defined structure of the pores, ion exchange capability, and variety of surface properties make zeolites ideal systems for imaginative host−guest chemistry aimed at the preparation of novel catalysts.[5] Recent examples of such systems include the assembly of organometallic complexes in the zeolite pores from preadsorbed precursors, for example, with Os−Carbonyl clusters,[6] the formation of $[Ir_6(CO)_{15}]^{2-}$ in NaX from preadsorbed $[Ir(CO)_2(acac)]$ treated with CO,[7] or palladium carbonyl clusters in NaY.[8]

We have developed a concept for stabilizing low-valent transition metal moieties (such as $Cl_2(THF)GeMo(CO)_5$[9] or $Me_3SnMn(CO)_5$[10]) in large-pore zeolites, by using bimetallic complexes where the second, oxophilic main-group element serves to attach the complex to the internal zeolite cage surface. The protons located at the zeolite Si−O−Al bridges are highly acidic. These hydroxyls represent an attractive, largely unexplored type of reactive site for attaching organometallic fragments. Since small species can be anchored, pore clogging can be avoided, and a homogeneous site distribution is likely.

This approach differs from other strategies such as physisorption of neutral metal carbonyls,[11] diffusional blocking of phthalocyanine and other chelate complexes,[12] and ligation at transition metal cations such as formation of Rh carbonyl complex cations.[13] Improved stability of intrazeolite species should be expected from surface-attached complexes that utilize the bridging zeolite hydroxyls for anchoring reactions, such as $Rh(allyl)_3$ in partially proton-exchanged X and Y type zeolite.[14]

In this article we discuss the surface chemistry and stability of $Me_3SnCo(CO)_4$ in different acidic Y type supports. The reactivity of the SnCo complex and the stability of the Sn−Co bond under different conditions have been explored.[15] Reaction with phosphines leads exclusively to monosubstituted products in the trans position to $Me_3Sn$.[16] Heterolytic cleavage of the Sn−Co bond and recombination are possible in certain ionizing solvents such as DMF[17] and acetone.[18] The precursor is expected to react with the internal surface hydroxyl groups of the zeolites by loss of methane gas whereas the Sn−Co bond and the coordination sphere of Co should remain intact under certain conditions.

A comprehensive combination of analytical techniques has been used to probe local structural changes at the molecular level. These techniques include EXAFS (extended X-ray absorption fine structure) spectroscopy utilizing synchroton radiation and *in situ* FTIR coupled to thermodesorption.

## Experimental Section

**Sample Preparation.** All manipulations were carried out under nitrogen atmosphere, and nitrogen-saturated solvents were distilled from appropriate drying agents. The precursor $Me_3SnCo(CO)_4$ (mp 73−74 °C, $^1$H-NMR: 0.63 ppm in $CDCl_3$, $J(^{119}Sn-H) = 52.6$ Hz, $J(^{117}Sn-H) = 50.6$ Hz) was synthesized from the reaction between $Co_2(CO)_8$ and $Me_3SnCl$ in MeOH following a modified reported method.[19] The SnCo complex was purified by vacuum sublimation prior to use.

The precursor was immobilized into acidic forms of zeolite Y, denominated H6Y (6 $H^+$/sc), obtained from Linde LZ-Y62 $[(NH_4)_{45}Na_{10}Al_{55}Si_{137}O_{384}]\cdot 235H_2O$, and H2Y, obtained from stoichiometric ammonium exchange of NaY zeolite at 80 °C for 4 h (commercial PQ Valfor CBV 100 $[Na_{54}Al_{54}Si_{138}O_{384}]\cdot 235H_2O$). Heating the ammonium-exchanged zeolite under

* Author for correspondence.

® Abstract published in *Advance ACS Abstracts,* November 15, 1994.

0022-3654/94/2098-13651$04.50/0 

oxygen flow at 100 °C for 4 h and at 400 °C for 8 h and then under vacuum at the same temperature for 6 h (at a rate of 1 °C/min) resulted in the desired acid form. The dehydrated zeolites were kept in sealed vials in a glovebox prior to further treatments. An amount of 0.500 g of each zeolite was loaded with 1.1 molecule/supercage of $Me_3SnCo(CO)_4$ in 50 mL of dry hexane by stirring the slurry for 18 h under dry nitrogen atmosphere. The yellowish solution was decolorized after impregnation. The slurry was filtered and washed several times with pentane. The intrazeolite samples were dried at $10^{-4}$ Torr for 1 h. X-ray fluorescence measurements showed the expected loading levels (1.0 ± 0.2 molecule per supercage); thus, loading was nearly quantitative.

The structural features of the intrazeolite SnCo species were determined by EXAFS spectroscopy at both the Co edge and Sn edge. EXAFS samples were prepared by heating 0.500 g batches of loaded zeolites in a tube furnace between 90 and 300 °C under vacuum ($10^{-5}$ Torr; heating rate 1 °C/min). The samples were kept at the desired temperature for 6 h. The powdered samples were mixed with a molten, degassed 1:1 mixture of octadecane and eicosane at 30–35 °C, and the encapsulated samples were packaged in EXAFS sample holders, sealed with Kapton tape, and kept under nitrogen until EXAFS measurements were performed. Our previous studies indicate that this technique precludes air oxidation (see ref 9). Powder X-ray diffraction shows that the samples remain crystalline after the heat treatments.

**Characterization.** FTIR data of thin zeolite dispersions on Si wafers in a steel cell with heating block were taken with a Mattson Polaris spectrometer at 4 $cm^{-1}$ resolution. The samples were evacuated with a molecular sieve/turbomolecular pump combination until the total pressure (including $H_2$) was $<10^{-6}$ Torr prior to any treatment. Zeolite samples were heated at 2 °C/min while FTIR and mass spectra were monitored. Electronic spectra were obtained in the diffuse reflectance mode with an integrating sphere in an Hitachi 3501 UV–near-IR spectrometer. X-ray fluorescence provided elemental composition of the samples (Sn, Co).

EXAFS measurements were carried out at NSLS (Brookhaven National Laboratories) at beamline X-11A with a stored energy of 2.5 GeV and ring currents between 100 and 200 mA. Data were collected at the Co K edge (7709 eV) and the Sn K edge (29 200 eV). The experiments were performed at about 100 K in transmission using a double crystal Si(311) monochromator. The EXAFS data were analyzed using standard procedures, as described in a previous article.[10] Fourier transform ranges ($k^3$-weighted) were chosen close to 2.5–11.0 $Å^{-1}$.

To evaluate the carbonyl ligation at the cobalt edge, the C and O components of the carbonyl ligands were fitted with the respective contribution in $Ni(CO)_4$. The metal–metal bond (Co–Sn) is partially obscured by the carbonyl ligands. After subtracting the calculated CO backscattering from the original data, the remaining amplitude function is similar to a heavier metal backscatterer. This function was used as internal reference for the zeolite samples for the metal–metal bond. A combined fit of the carbon- and metal shells gave the final results. The tin EXAFS data were fitted with $SnMe_4$ and $Me_3SnMn(CO)_5$ as reference for the Sn–C/O and Sn–metal bonds, respectively. (No X-ray structure is available for $Me_3SnCo(CO)_4$.)

## Results and Discussion

**$Me_3SnCo(CO)_4$ in HY Zeolite.** The complex–surface interactions and the thermal stability of the encapsulated complex were studied with *in-situ* infrared spectroscopy coupled with temperature-programmed desorption.

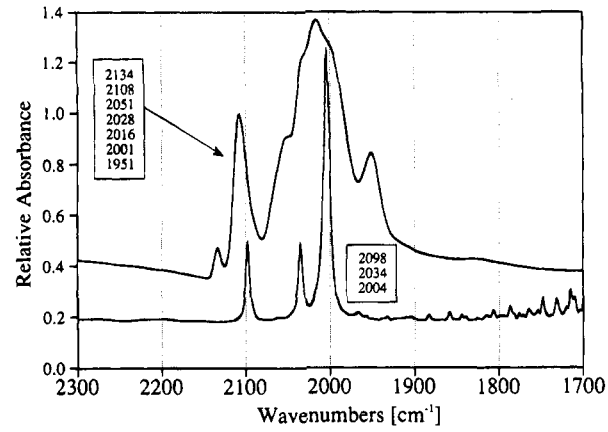


**Figure 1.** Infrared spectra of the carbonyl stretching region of $Me_3SnCo(CO)_4$ in H6Y (A) compared with the precursor in Fluorolube mull (B).

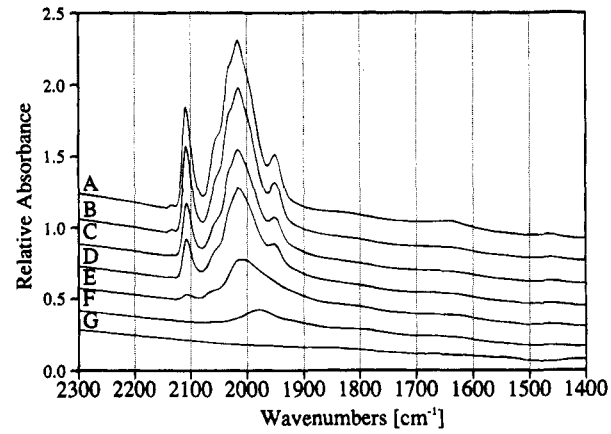


**Figure 2.** *In-situ* FTIR spectra of $Me_3SnCo(CO)_4$ in the H6Y host under vacuum: A, 30; B, 100; C, 120; D, 130; E, 150; F, 190; G, 300 °C. Heating rate 2 °C/min.

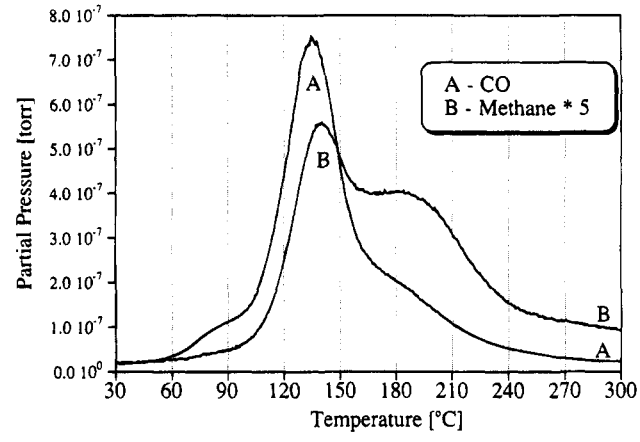


**Figure 3.** TPD/MS data of $Me_3SnCo(CO)_4$ in the H6Y host, heated under vacuum at a heating rate of 2 °C/min. (A) CO (*m/e* = 28). (B) $CH_4$ (*m/e* = 16). The methane signal is 5× enlarged.

When the tin–cobalt complex is absorbed into the H6Y host, an increased number of bands and a moderate shift of major bands to higher energies is observed in the CO stretching region (major peaks among at least seven listed in Figure 1: 2108 and 2016 $cm^{-1}$, compared to Fluorolube data: 2098, 2034, and 2004 $cm^{-1}$ (in hexane: 2083, 2020, and 1988 $cm^{-1}$)). This shift is indicative of a possible substitution of one or more methyl ligands by the zeolite oxygen framework (see EXAFS data below), similar to the reaction observed with $Me_3SnMn(CO)_5$.[10] We note that the CO stretch modes of $Cl_3SnCo(CO)_4$ occur at

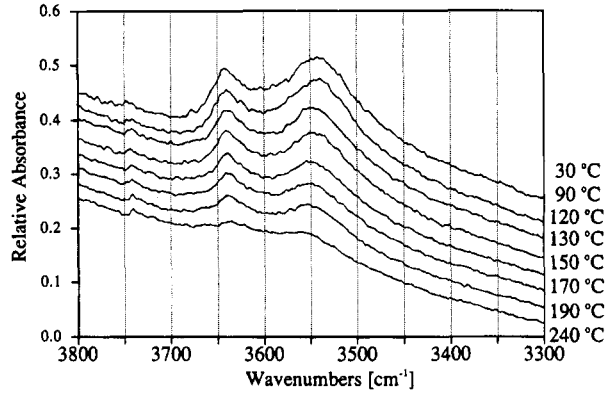


**Figure 4.** *In-situ* infrared data of the hydroxyl region of $Me_3SnCo(CO)_4$ in the H6Y host, heated to the temperatures given in the figure.

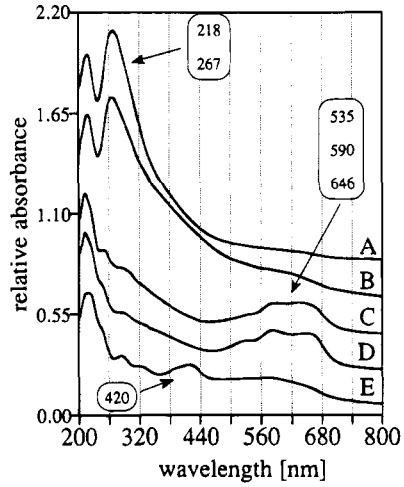


**Figure 5.** UV/vis spectra of $Me_3SnCo(CO)_4$ in H6Y, after different heat treatments under vacuum (batch treatment as for the EXAFS samples; see text): A, 30; B, 90; C, 160; D, 190; E, 300 °C.

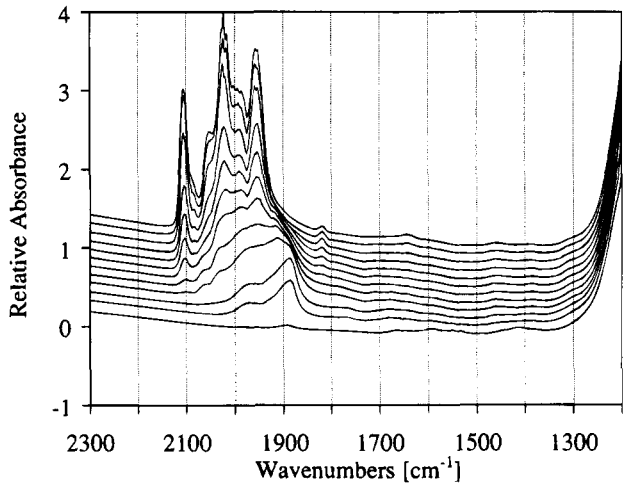


**Figure 6.** *In-situ* FTIR spectra of $Me_3SnCo(CO)_4$ in the H2Y host under vacuum, heated (from top) to 41, 87, 116, 135, 145, 155, 181, 201, 227, 255, 286, and 328 °C. Heating rate 2 °C/min.

higher frequencies (2120, 2068, and 2048 $cm^{-1}$) than those of the $Me_3Sn$ derivative.[20] The spectrum in the acidic host is different from the corresponding one in the nonacidic form NaY,[21] because only a small number of sodium ions are available for association with the carbonyl ligands. The presence of other potential products, such as $Co(CO)_4^-$ (1886 $cm^{-1}$ in THF) or $HCo(CO)_4$ (2116, 2053, and 2030 $cm^{-1}$ in hexane),[22] is considered unlikely because the peak positions differ significantly from the encapsulated SnCo complex. The

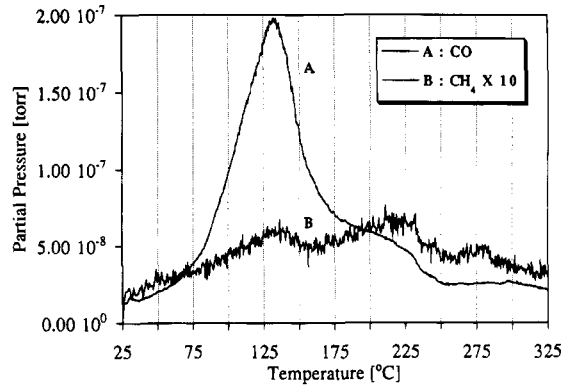


**Figure 7.** TPD/MS data of $Me_3SnCo(CO)_4$ in the H2Y host, heated under vacuum at a heating rate of 2 °C/min. Species are given in the figure.

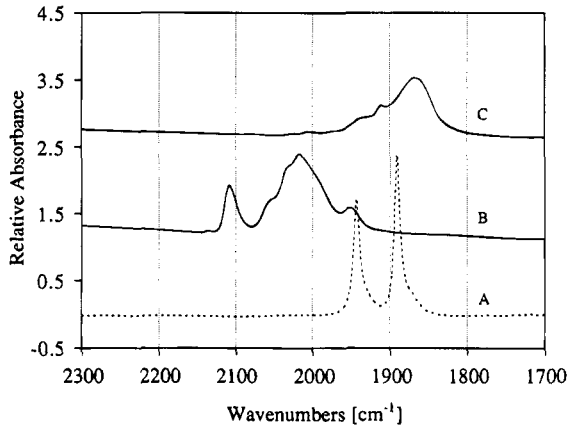


**Figure 8.** Reactivity of $Me_3SnCo(CO)_4$ with $PMe_3$: (A) $Me_3SnCo(CO)_3(PMe_3)$ synthesized in solution; (B) $Me_3SnCo(CO)_4$ in zeolite H6Y; (C) $Me_3SnCo(CO)_4$ in zeolite H6Y treated with $PMe_3$.

**TABLE 1: Structural Results for $Me_3SnCo(CO)_4$ in H6Y Derived from EXAFS Data**

| sample | atom pair | $N^a$ | $R$/Å$^b$ | $\Delta\sigma^2$/Å$^{2\,c}$ | $\Delta E$/eV$^d$ |
|---|---|---|---|---|---|
| RT | Co–CO | 4.2 | 1.78 | 0.0001 | 1.2 |
| | Co–$\overline{CO}$ | 4.7 | 2.96 | −0.0008 | −0.5 |
| | Co–Sn | *ca.* 1 | 2.68 | | |
| | Sn–C/O | 3 | 2.13 | 0.0045 | 1.5 |
| | Sn–Co | *ca.* 1 | 2.55 | | |
| 90 °C$^f$ | Co–CO | 3.7 | 1.73 | 0.0074 | 4.8 |
| | Co–$\overline{CO}$ | 3.6 | 2.91 | −0.0002 | −1.0 |
| | Co–Sn | *ca.* 1 | 2.64 | | |
| 160 °C | Co–$O_z$$^d$ | 1.8 | 2.06 | −0.0025 | −2.9 |
| | Sn–$O_z$ | 2.9 | 2.12 | 0.0096 | 3.7 |
| 190 °C | Co–$O_z$ | 4.6 | 2.07 | 0.0049 | −2.9 |
| | Sn–$O_z$ | 3.3 | 2.15 | 0.012 | 3.3 |
| 300 °C | Co–$O_z$ | 3.7 | 2.05 | 0.0021 | 0.07 |

$^a$ Coordination number. $^b$ Bond distance. $^c$ Static disorder. $^d$ Inner potential. $^e$ $O_z$ = zeolite framework oxygen. $^f$ Sn-edge data similar to RT but no unique fits were obtained.

volatile hydrido complex is not expected to remain in the H6Y host under high vacuum at elevated temperature.

The reactivity of the SnCo complex in proton-containing zeolite H6Y is quite different from that in NaY, where alloy cluster formation is observed.[21] Figure 2 shows the *in-situ* IR spectra of the thermal decomposition of the carbonyl moiety in H6Y. In contrast to the NaY system, the carbonyl pattern does not change much except for a simultaneous decrease in intensity. A small broad band remains at *ca.* 2000 $cm^{-1}$, which shifts to lower energy until all CO ligands are lost at 300 °C under these dynamic conditions. Apparently, no clusters with bridging CO ligands are formed. These data show that the zeolite-attached

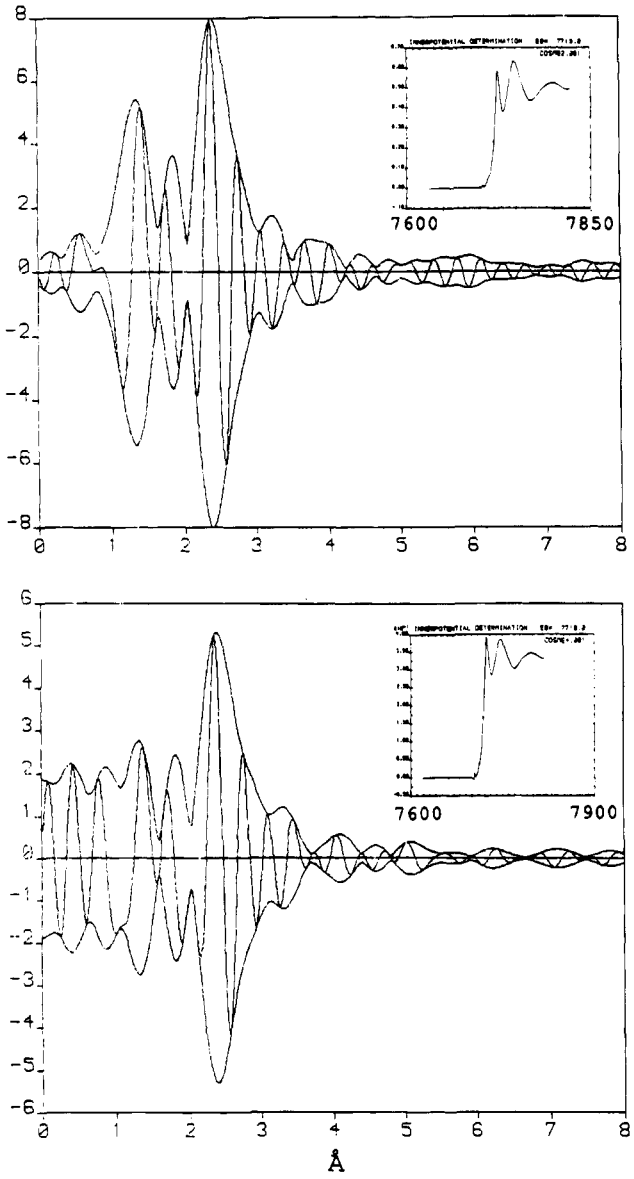


**Figure 9.** Fourier-transformed EXAFS data of $Me_3SnCo(CO)_4$ in H6Y at different treatment temperatures, Co edge: top, 30 °C; bottom, 90 °C. Abscissa: distance in Å. Inserts: edge structures, from 7600 to 7850 eV (top) and from 7600 to 7900 eV (bottom).

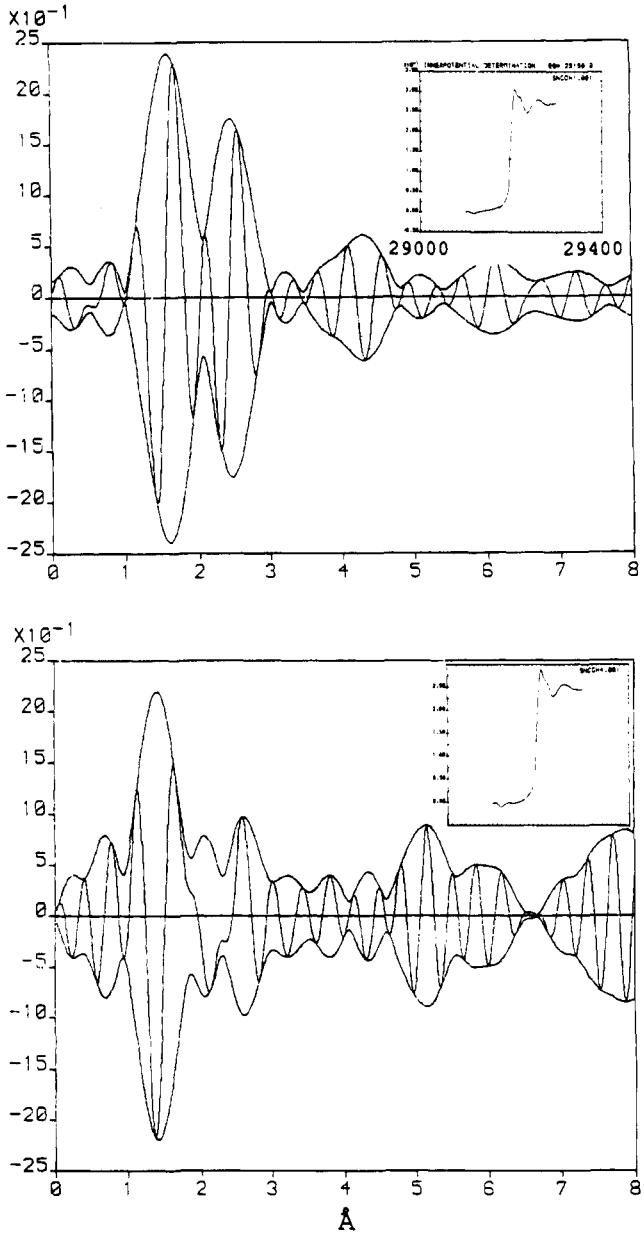


**Figure 10.** Fourier-transformed EXAFS data of $Me_3SnCo(CO)_4$ in H6Y at different treatment temperatures, Sn edge: top, 30 °C; bottom, 90 °C. Abscissa: distance in Å. Inserts: edge structures, from 29 000 to 29 400 eV.

species are decomposed at lower temperature than in the NaY host where the CO evolution peaks at 150 °C. (Minor loss of CO in H6Y begins at 60 °C and peaks at 130 °C, and significant loss of methane occurs at 120 °C; see thermodesorption data in Figure 3.) The methane evolution occurs in two steps (maxima at 140 and 180 °C), suggesting stepwise reaction of the methyl ligands of the $SnMe_3$ moiety with the zeolite hydroxyl groups. The continued consumption of the zeolite hydroxyl groups up to temperatures above 240 °C can be observed in the hydroxyl stretching region (Figure 4).

The UV/vis region (measured in diffuse reflectance, Figure 5) of the SnCo complex in H6Y at different temperatures shows complete destruction of the carbonyl-related charge-transfer band at 267 nm on heating to 160 °C. Three new bands at 535, 590, and 646 nm are observed at the same temperature, indicating that cobalt has been oxidized to Co(II) by the acidic zeolite and that it now coordinates to the zeolite framework in a pseudotetrahedral geometry. The above bands coincide with those observed when dehydrating Co(II)-exchanged zeolite Y at 300 °C.[23] In the latter study it was suggested that the fourth ligand (in addition to three framework oxygens from a 6-ring) could be oxygen or hydroxide or represented by the field of the sodalite cavity. On heating to 300 °C, the SnCo system shows a new band at 420 nm that could be associated with trigonal-planar Co coordination.[23] These spectral changes confirm our EXAFS data, where the average Co−O coordination drops by about one ligand on heating to 300 °C (see below).

**Adsorption in H2Y Host.** When the SnCo complex is adsorbed into the H2Y host, we observe a strong CO stretch band at 1960 $cm^{-1}$ in addition to the pattern observed for H6Y (Figure 6). The new band is related to Na-associated $Me_3SnCo(CO)_4$, where carbonyl ligands interact with the Lewis acidic sodium ions according to Na- -OC−Co. This assignment is based on the dominant peak at similar position observed when the complex resides in NaY.[21] *In-situ* IR measurements of the decomposition pathway in H2Y reveal that species with a low-energy carbonyl stretch of similar energy as in NaY are formed, suggesting the growth of very small carbonyl-decorated clusters (Figure 6). The TPD/MS data of this system show CO evolution peaking at 130 °C and only little methane production (Figure

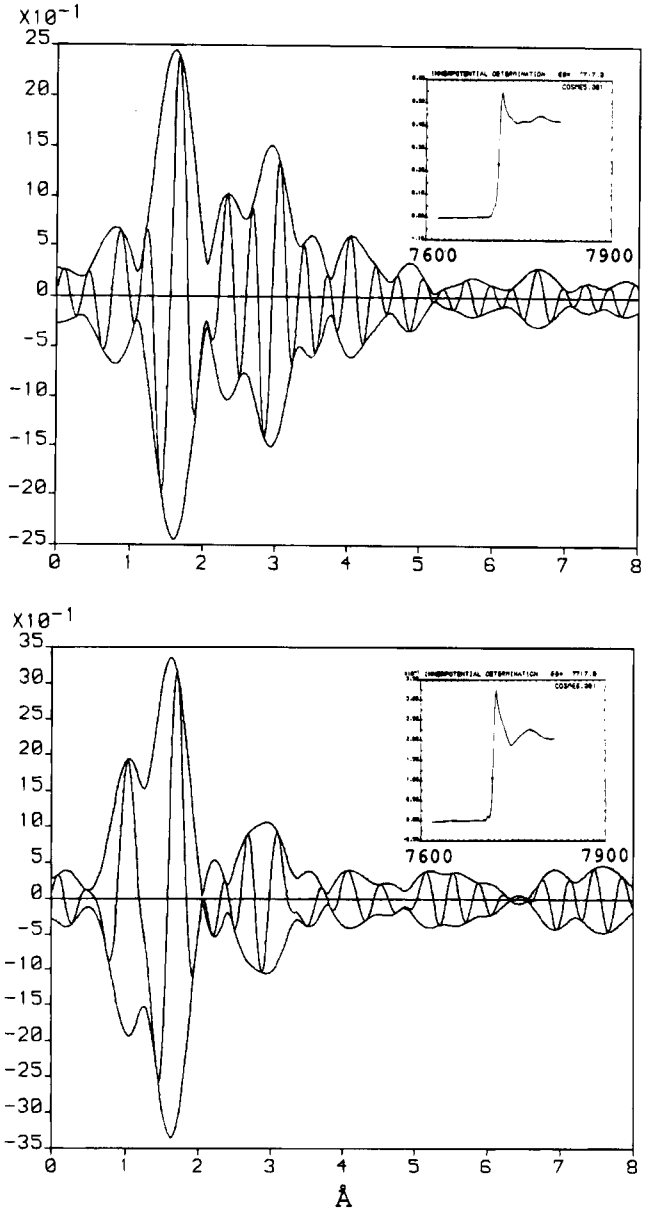


**Figure 11.** Fourier-transformed EXAFS data of $Me_3SnCo(CO)_4$ in H6Y at different treatment temperatures, Co edge: top, 160 °C; bottom, 190 °C. Abscissa: distance in Å. Inserts: edge structures, from 7600 to 7900 eV.

7). Taken together, these data suggest that the lower number of protons available per complex (a maximum of 2 *vs* 6 in H6Y) leads to a profound change in intrazeolite surface reactivity. The complex can attach to the zeolite via one or two Si−O−Sn bridges, but oxidation of cobalt cannot take place; thus, metal clusters can form at higher temperature.

**Chemical Reactivity of the Sn−Co Precursor in H6Y Zeolite.** The reactivity of trimethylphosphine with the encapsulated SnCo complex was studied in comparison to the solution reaction. The latter was carried out under nitrogen by stirring 1:5 molar ratios of complex:$PMe_3$ for 12 h at 70 °C in THF. The product shows two strong infrared CO stretching modes (1943 and 1891 $cm^{-1}$ in hexane; 1936 and 1880 $cm^{-1}$ in THF), compared with the three modes of the precursor at 2083, 2020, and 1988 $cm^{-1}$. The new IR pattern is typical for increased $\pi$-backbonding on substitution of carbonyls with phosphine, and together with NMR data it is consistent with the exclusive formation of monosubstituted $Me_3SnCo(CO)_3(PMe_3)$ (Figure 8).

The reaction of $PMe_3$ with the encapsulated SnCo complex in H6Y was carried out in a Schlenk flask. A vial with a 3-fold excess of the phosphine relative to the SnCo complex was connected to an evacuated flask containing SnCo−zeolite. The phosphine was heated to 80 °C and was then allowed to expand into the flask. Subsequently, the flask was closed and heated for 48 h at 70 °C, and the sample was evacuated and washed with pentane after cooling to remove excess phosphine. The CO stretch pattern shows drastic changes after this reaction. The original bands in H6Y (major peaks at 2108, 2016, and 1951 $cm^{-1}$) are replaced by a broader peak at 1868 $cm^{-1}$ with a shoulder at 1911 $cm^{-1}$. This red shift is consistent with phosphine substitution and increased $\pi$-backbonding, as in the solution reaction (Figure 8). These results show that the intrazeolite complex $Me_3SnCo(CO)_4$ can react with a phosphine ligand diffusing into the pore system. Thermal desorption of the more stable phosphine-substituted product in the H6Y host (3 °C/min heating rate) shows phosphine evolution at 150 °C, due to desorption of excess $PMe_3$, and complex decomposition accompanied by evolution of phosphine and CO at about 190 °C.

The EXAFS analysis shows that the cobalt carbonyl coordination sphere remains intact on introduction of the complex

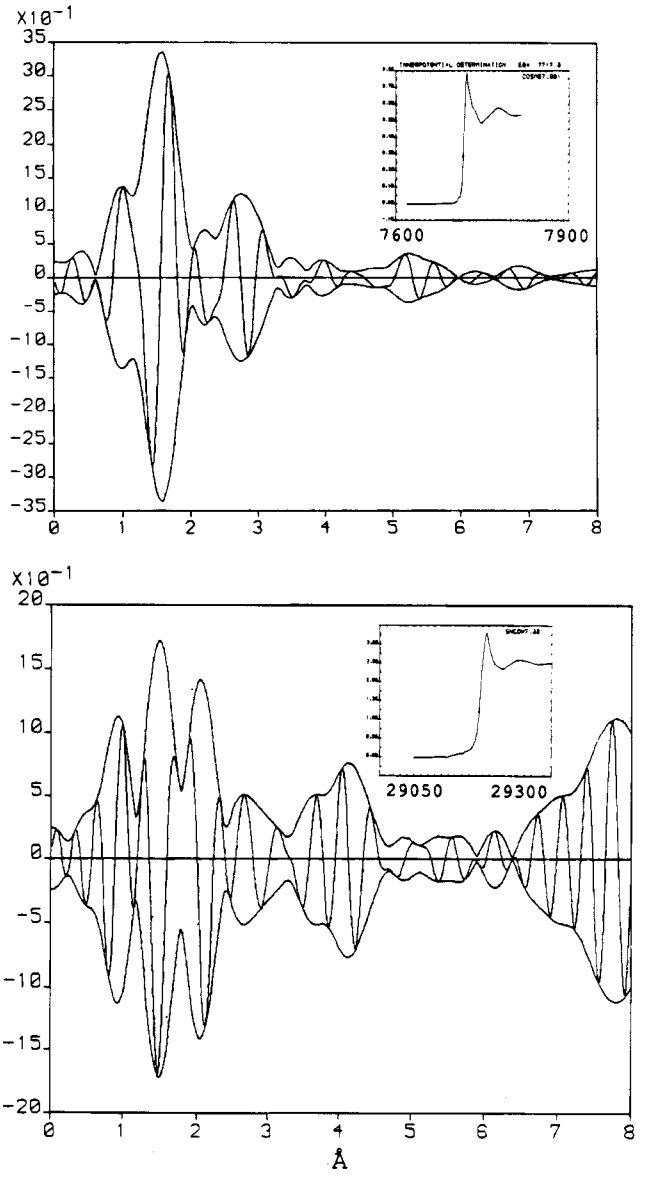


**Figure 12.** Fourier-transformed EXAFS data of $Me_3SnCo(CO)_4$ in H6Y heated to 300 °C: top, Co edge; bottom, Sn edge. Abscissa: distance in Å. Inserts: edge structures, from 7600 to 7900 eV (top) and from 29 050 to 29 300 eV (bottom).

into the acidic H6Y zeolite at room temperature (Co−CO, 4.2 ligands at 1.78 Å; Co−CO, 4.7 at 2.96 Å). The Co−Sn bond is detected at 2.68 Å, when using a Sn−Mn reference for the fit (Figure 9, Co edge; Figure 10, Sn edge; Table 1). We note that the coordination number for the Co−Sn bond cannot be determined reliably because of significant overlap with the oxygen shell. At the tin edge, a total of three carbon/oxygen ligands at 2.13 Å is observed. In comparison with tin edge data in the NaY host (not shown), the tin edge of the SnCo complex in H6Y indicates that some of the carbon is already replaced by zeolite oxygen, which implies chemical attachment to the zeolite framework. No zeolite framework metal is detected, probably a result of disorder in the weakly zeolite-associated state of the tin−cobalt complex at low temperature. In addition to the first tin shell, a well-separated second shell due to the Sn−Co bond is observed. The corresponding Sn−Co distance, 2.55 Å, appears to be 0.13 Å shorter than that obtained at the cobalt edge, probably because optimal reference EXAFS data for this bond are not available and because of overlapping shells at the Co edge.

On heating to 90 °C, the cobalt carbonyl sphere remains largely intact (Co−CO, 3.7 ligands at 1.73 Å; Co−CO, 3.6 at 2.91 Å; Figures 9 and 10), and the Co−Sn bond is again observed at 2.64 Å. The tin edge shows further reduction of carbon features, and the tin−carbon/oxygen coordination appears now more disordered (no unique fits were obtained), suggesting a greater degree of oxygen substitution and attachment to the zeolite framework. This is supported by the evolution of methane in the IR/TPD-MS experiment (Figure 3).[24]

Drastic changes occur between 90 and 160 °C, notably the removal of most of the carbonyl ligands, appearance of Co−O coordination (Co−$O_{1.8}$ at 2.06 Å), and a strong indication for coordination of Co to the zeolite framework: A new shell emerges at 3 Å in the radial distribution function (Figure 11). The drastic decarbonylation in this temperature range is confirmed in the IR/TPD-MS experiments discussed above (see Figure 3 for mass spectrometric data). The above trends continue on heating to 190 °C: Complete dissociation of CO (the Co edge shows complete removal of the CO-based feature that was seen at RT and 90 °C), significant Co−$O_z$ coordination (4.6 $O_z$ at 2.07 Å; $O_z$ = zeolite oxygen), and zeolite−framework backscattering are observed. (The outer shell cannot be fitted with Co backscattering and is believed to be due to Si/Al.)

The evolution of the cobalt coordination at elevated temperatures signals a reactivity of the SnCo complex in H6Y that is very different from that in the nonacidic NaY host. In the latter, small metal alloy clusters are formed at 300 °C. In contrast, the H6Y host provides enough protons (*ca.* 6 per complex) for complete removal of methyl ligands at tin and for the oxidative decarbonylation of the cobalt moiety, leading to framework-attached Co(II). Accordingly, no cluster formation is detected at 300 °C in H6Y. Instead, we observe Co−$O_z$ coordination (3.7 at 2.05 Å), very similar to that of ion-exchanged and calcined cobalt(II) in zeolite Y, reported previously to occur at 2.07 Å (Figure 12),[25] and outer-shell zeolite scattering. Thus, on heating the sample to 190 and 300 °C, the cobalt moves into close coordination with the zeolite framework. The cobalt−oxygen coordination (about four oxygen ligands at 2.05 Å) is typical for cobalt ions positioned at zeolite coordination sites such as SII. Furthermore, neither Co−Co nor Sn−Sn scattering is detected, but the tin fragments are now exclusively coordinated to oxygen as derived from the tin edge. The apparent presence of several Sn−O coordination distances makes a reliable analysis difficult, but it indicates a range of local coordination numbers and possibly different tin−oxo species (Figure 12). At high temperatures, the acidic host thus leads to oxidative decarbonylation and cleavage of the tin−cobalt complex, to form cobalt ions attached to the zeolite framework.

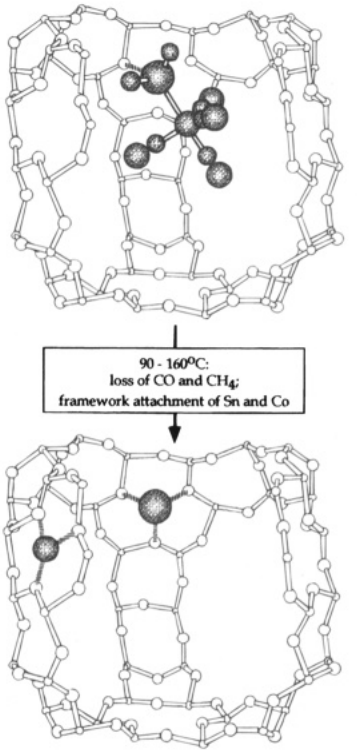


**Figure 13.** Intrazeolite chemistry of $Me_3SnCo(CO)_4$ in zeolite H6Y.

## Conclusions

The combination of EXAFS data and *in-situ* FTIR coupled with TPD-MS measurements discussed above provides a comprehensive picture of the intrazeolite structure and chemistry of $Me_3SnCo(CO)_4$ in the acidic zeolite Y containing an average of six protons per supercage (Figure 13).

The H6Y host offers a chemically reactive surface that can interact with the $Me_3Sn$ moiety of the bimetallic complex. Increasing degrees of substitution of the methyl groups by the oxygen framework are observed. The degree of substitution increases with temperature. The Sn−Co bond is cleaved between about 90 and 160 °C, and oxidative decarbonylation of Co leads to Co(II) attached to the zeolite framework with pseudotetrahedral coordination.

These results show that the heterobimetallic compound $Me_3SnCo(CO)_4$ can be anchored into the cages of acidic zeolites at room temperature under retention of the Sn−Co bond. The methyl ligands are good leaving groups in H6Y. The intrazeolite complex in H6Y is accessible toward carbonyl substitution with $PMe_3$ at the cobalt atom.

In comparison with the very different reactivity of the same precursor complex in nonacidic NaY, these results show that the intrazeolite chemistry and reactivity can be controlled by the choice of host reactivity, i.e., the number of acidic protons lining the host cages. The interplay of host reactivity and precursor structure and reactivity allows us to produce a wide range of intrazeolite species with potential as selective catalysts and other materials with interesting functionality.

**Acknowledgment.** The authors thank Professor D. C. Koningsberger for software used in the EXAFS data analysis. Funding from the U.S. Department of Energy for this work

is gratefully acknowledged. The operational funds for NSLS beamline X-11A are supported by DOE Grant DE-AS0580ER10742.

## References and Notes

(1) (a) Gates, B. C.; Guczi, L.; Knözinger, H. *Metal Clusters in Catalysis*; Elsevier: Amsterdam, 1986. (b) Basset, J.-M., Gates, B. C., Candy, J. P., Choplin, A., Leconte, M., Quignard, F., Santini, C., Eds. *Surface Organometallic Chemistry: Molecular Approaches to Surface Catalysis*; Kluwer: Dordrecht, 1988. (c) Basset, J.-M.; Candy, J. P.; Choplin, A.; Santini, C.; Theolier, A. *Catal. Today* **1989**, *6*, 1. (d) Lamb, H. H.; Gates, B. C.; Knözinger, H. *Angew. Chem., Int. Ed. Engl.* **1988**, *27*, 1127. (e) Yermakov, Yu. I.; Kuznetsov, B. N.; Zakharov, V. A. *Catalysis by Supported Metal Complexes*; Elsevier: Amsterdam, 1981. (f) Bailey, D. C.; Langer, S. H. *Chem. Rev.* **1981**, *81*, 109. (g) Ozin, G. A.; Gil, C. *Chem. Rev.* **1989**, *89*, 1749–64. (h) Ozin, G. A.; Ozkar, S. *Chem. Mater.* **1992**, *4*, 511–21.

(2) Hartley, F. R. *Supported Metal Complexes*; D. Reidel: Dordrecht, 1985.

(3) (a) Breck, D. W. *Zeolite Molecular Sieves*; R. E. Krieger Publishing: Malabar, FL, 1984. (b) *Zeolites: Facts, Figures, Future*; Jacobs, P. A., van Santen, R. A., Eds.; Stud. Surf. Sci. Catal. 49; Elsevier: Amsterdam, 1989.

(4) (a) Davis, M. E.; Lobo, R. F. *Chem. Mater.* **1992**, *4*, 756–68. (b) Suib, S. L. *Chem. Rev.* **1993**, *93*, 803–26. (c) *Introduction to Zeolite Science and Practice*; van Bekkum, H., Flanigen, E. M., Jansen, J. C., Eds.; Elsevier: Amsterdam, 1991. (d) Jacobs, P. A. *Carboniogenic Activity of Zeolites*; Elsevier: Amsterdam, 1977.

(5) Sachtler, W. M. H.; Zhang, Z. Adv. Catal. **1993**, *39*, 129–220.

(6) Zhou, P. L.; Maloney, S. D.; Gates, B. C. *J. Catal.* **1991**, *129*, 315–29.

(7) Kawi, S.; Gates, B. C. *Chem. Commun.* **1992**, 702–3.

(8) Sachtler, W. M. H.; Zhang, Z. *Adv. Catal.* **1993**, *39*, 129–220, Chapter III.

(9) (a) Borvornwattananont, A.; Moller, K.; Bein, T. *J. Chem. Soc., Chem. Commun.* **1990**, 28. (b) Borvornwattananont, A.; Moller, K.; Bein, T. In *Synthesis/Characterization and Novel Applications of Molecular Sieve Materials*; Bedard, R. L., Bein, T., Davis, M. E., Garces, J., Maroni, V. A., Stucky, G. D., Eds.; *Mater. Res. Soc. Symp. Proc.* **1991**, *233*, 195. (c) Borvornwattananont, A.; Moller, K.; Bein, T. *J. Phys. Chem.* **1992**, *96*, 6713.

(10) Borvornwattananont, A.; Bein, T. *J. Phys. Chem.* **1992**, *96*, 9447.

(11) (a) Suib, S. L.; Kostapapas, A.; McMahon, K. C.; Baxter, J. C.; Winiecki, A. M. *Inorg. Chem.* **1985**, *24*, 858. (b) Bein, T.; McLain, S. J.; Corbin, D. R.; Farlee, R. F.; Moller, K.; Stucky, G. D.; Woolery, G.; Sayers, D. *J. Am. Chem. Soc.* **1988**, *110*, 1801.

(12) (a) Herron, N. *Inorg. Chem.* **1986**, *25*, 4714. (b) Diegruber, H.; Plath, P. J.; Schulz-Ekloff, G. *J. Mol. Catal.* **1984**, *24*, 115.

(13) (a) Davis, M. E.; Schnitzer, J.; Rossin, J. A.; Taylor, D.; Hanson, B. E. *J. Mol. Catal.* **1987**, *39*, 243. (b) Shannon, R. D.; Vedrine, J. C.; Naccache, C.; Lefebvre, F. *J. Catal.* **1984**, *88*, 431. (c) Rode, E. J.; Davis, M. E.; Hanson, B. E. *J. Catal.* **1985**, *96*, 574.

(14) (a) Huang, T. N.; Schwartz, J.; Kitajima, N. *J. Mol. Catal.* **1984**, *22*, 389. (b) Huang, T. N.; Schwartz, J. *J. Am. Chem. Soc.* **1982**, *104*, 5244. (c) Corbin, D. R.; Seidel, W. C., Abrams, L.; Herron, N.; Stucky, G. D.; Tolman, C. A. *Inorg. Chem.* **1985**, *24*, 1800. (d) Taylor, D. F.; Hanson, B. E.; Davis, M. E. *Inorg. Chim. Acta* **1987**, *128*, 55.

(15) (a) King, R. B. *J. Mol. Catal.* **1981**, *10*, 75. (b) King, R. B.; King, A. D. J.; Tanaka, K. *J. Mol. Catal.* **1980**, *10*, 75–83. (c) Absi, H. M.; Brown, T. L. *J. Am. Chem. Soc.* **1977**, *99*, 2982–8. (d) Chipperfield, J. R.; Hayter, A. C.; Webster, D. E. *J. Organomet. Chem.* **1976**, *121*, 185–8. (e) Clark, H. C. *J. Organomet. Chem.* **1968**, *11*, 601.

(16) (a) Brown, T. L.; Ogino, K. *Inorg. Chem.* **1971**, *10*, 517–21. (b) Schumann, H.; Feldt, W. *Z. Allg. Anorg. Chem.* **1979**, *458*, 257.

(17) Burlitch, J. M. *J. Am. Chem. Soc.* **1969**, *91*, 4562.

(18) Beveridge, A. D.; Clark, H. C. *J. Organomet. Chem.* **1968**, *11*, 601.

(19) Patmore, D. J.; Graham, W. A. G. *Inorg. Chem.* **1967**, *6*, 981.

(20) Patmore, D. J.; Graham, W. A. G. *Inorg. Chem.* **1968**, *7*, 771.

(21) Huber, C.; Moller, K.; Bein, T. *J. Phys. Chem.*, in press.

(22) Braterman, P. S. *Metal Carbonyl Spectra*; Academic Press: London, 1975.

(23) Hutta, P. J.; Lunsford, J. H. *J. Chem. Phys.* **1977**, *66*, 4716–7.

(24) We note that the EXAFS sample preparations in batch mode with long isothermal heating do not allow us a direct comparison with intrazeolite reactions observed in TPD/MS experiments at the same nominal temperature, where the sample is presented in a very thin layer and the temperature is continuously ramped.

(25) Moller, K.; Bein, T. *Zeolites: Facts, Figures, Future*; Jabobs, P. A., Van Santen, R. A., Eds.; Elsevier: Amsterdam, 1989; pp 985–994.